Fourth-order relaxation processes in crystalline CO_2

Vijay K. Jindal,* Roberto Righini, and Salvatore Califano
Dipartimento di Chimica, Università degli Studi di Firenze, via Gino Capponi 9, I-50121 Firenze, Italy
(Received 30 March 1988)

The present work reports the results of a calculation of the phonon linewidths in solid CO_2, in which the anharmonic terms up to λ^4 in the perturbative series have been included. The aim has been that of interpreting the observed nonlinear temperature dependence of the linewidths of the Raman-active phonons and to learn about the processes responsible for their relaxation. It turns out that the adopted intermolecular potential, whose parameters were fitted to the low-temperature linewidths only, correctly predicts the temperature dependence of the linewidths up to 150 K. The role of the high-order terms of the perturbation series, in contrast with the general assumption, is not negligible at all; for temperatures above 40 K their contribution to the total linewidths is comparable to, and even larger than, that of the lowest-order term.

I. INTRODUCTION

The occurrence of finite widths for phonon bands in crystals is a direct consequence of the anharmonicity of the crystal potential. Anharmonicity introduces interactions between the otherwise dynamically independent phonons, which thermalize the phonon energy through phonon decay or induce pure dephasing processes, all contributing to the overall phonon relaxation.

The theory of phonon linewidths is a well-established many-body perturbation procedure.[1-6] In practice, however, linewidth calculations from anharmonic terms of the crystal Hamiltonian are extremely involved, mainly because of the complexity of the theoretical treatment, and of the time-consuming computational methods. This is particularly true for molecular crystals made of polyatomic molecules with a large number of interatomic interactions described by relatively complex analytical forms of potential.[5,6] For this reason such calculations have been performed only for a very limited number of molecular crystals[6] and, in any case, always to the lowest perturbative order. To this order (first order) the phonon relaxation is due to elementary three-phonon processes which either produce the decay of a phonon into two phonons of lower energy (down-conversion), or its fusion with another phonon of the thermal bath to produce a higher-energy phonon (up-conversion). The contribution of three-phonon processes to the phonon linewidth has a linear temperature dependence in the classical limit (high temperatures)—a result that follows directly from its linear dependence on the phonon occupation numbers. Calculation to this order is normally considered sufficient, especially when the measured linewidths show a linear temperature dependence in the high-temperature limit. Even if the temperature dependence is not linear at high temperatures, calculations to this order are always a useful first step for modification and refinement of the crystal potential, using the low-temperature data.

In an earlier paper,[7] a calculation of anharmonic phonon frequencies and bandwidths was made for crystalline CO_2 to the lowest order of anharmonicity of the crystal potential. Three different intermolecular potentials were utilized. The first (MOSMD), taken from an already existing calculation of harmonic phonon frequencies, includes atom-atom and quadrupole-quadrupole interactions. This potential turned out to be too anharmonic and produced physically unrealistic anharmonic corrections to the phonon frequencies as well as residual bandwidths at $T=0$ which are 1 order of magnitude larger than those observed. A second intermolecular potential (PRC-1) was derived from the previous one by shifting the oxygen interaction centers inside the C—O bond and by increasing the quadrupole moment. This second potential was much less anharmonic, giving rise to residual phonon bandwidths of the correct order of magnitude, although about twice larger than the experimental ones. An even less anharmonic potential (PRC-2) was then obtained by introducing a noncollinear distribution of negative charges around the bonds and refining the atom-atom interactions. The residual phonon bandwidths calculated with the PRC-2 potential were in perfect agreement with the experimental data. Owing to the fact that only three-phonon processes were considered, the calculated variation with temperature of the bandwidths has the expected linear dependence on T in the classical limit.

Recently very precise measurements[8] of the bandwidth of the three Raman-active lattice phonons of CO_2 (E_g, T_g^-, T_g^+) were made in a sufficiently broad range of temperature to evidentiate the type of law of evolution with T. It was found that in all three cases the bandwidths have a marked T^2 dependence which shows that higher-order processes play a significant role in the phonon relaxation.

It was therefore considered worthwhile to extend the bandwidth calculations, made with the previous potentials, by including the higher-order anharmonic terms. To our knowledge this is the first attempt ever made to include fourth-order processes in the calculation of phonon bandwidths for molecular crystals.

The present work is aimed to the calculation of these terms, which are several in number, each involving multiple Brillouin-zone (BZ) summations. Although formal

expressions are available[9,10] in the literature for the higher-order anharmonic terms, these are not always suitable for handling the numerical calculations. In Sec. II we give the formulas for evaluating the various contributions and we outline the numerical procedure used to estimate the bandwidths and the approximations made. Numerical calculations and results are presented and discussed in Sec. III.

II. THEORETICAL PROCEDURE

In perturbation theory the crystal Hamiltonian is expanded in powers[5]

$$H = H_0 + \lambda H_1 + \lambda^2 H_2 + \lambda^3 H_3 + \cdots , \tag{1}$$

where

$$H_0 = T + V_2$$

is the anharmonic Hamiltonian and $H_1, H_2, \ldots$ are perturbation terms whose magnitude is defined by the parameter λ. The generic perturbation term H_n of order n is defined as

$$H_n = \sum_{q_1,q_2,\cdots,q_n} V_n(q_1,q_2,\ldots,q_n) \times A(q_1)A(q_2)\cdots A(q_n) , \tag{2}$$

where $V_n(q_1,q_2,\ldots,q_n)$ is the Fourier transform of the nth expansion term of the crystal potential,[1-6] $A(q_n)=a^*(-q_n)+a(q_n)$ is a phonon operator expressed in terms of phonon creation, $a^*(q_n)$, and annihilation, $a(q_n)$, operators, and the index q is a collective symbol for the branch index j and for the phonon wave vector $\mathbf{k}$, $-q$ meaning $\{j,-\mathbf{k}\}$. Phonon bandwidths are normally obtained with the Green's-function technique by solving Dyson's equation for the phonon propagator $G_q(i\omega_m)$,

$$G_q(i\omega_m) \simeq G_q^0(i\omega_m) + G_q^0(i\omega_m) \sum_{q'} S_{q'}(i\omega_m) G_{q'}(i\omega_m) , \tag{3}$$

where m is an integer defined by the relation $\omega_m = 2\pi m/\beta\hbar$ with $\beta = 1/k_B T$, $G_q^0(i\omega_m)$ is the harmonic phonon propagator, and $S_{q'}(i\omega_m)$ is the phonon self-energy. For an optical phonon with wave vector $\mathbf{k}=0$, belonging to the j branch the half-bandwidth is given by the imaginary part of the self-energy

$$\Gamma_j(i\omega_m) = \mathrm{Im}[S_j(i\omega_m)] , \tag{4}$$

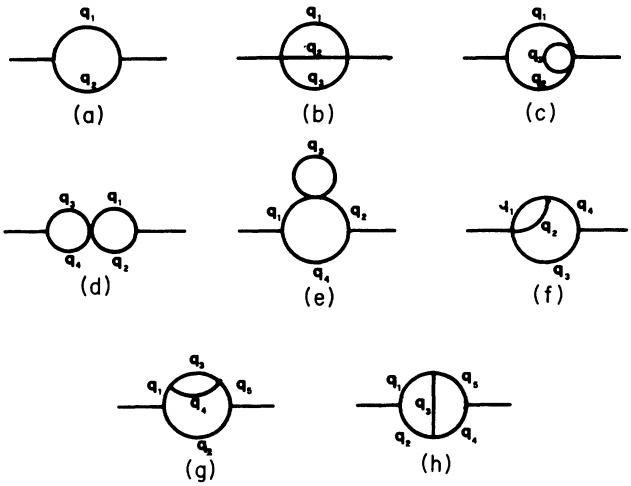

FIG. 1. Diagrammatic representation of the different terms of the perturbation series considered.

where for simplicity we have omitted the 0 wave-vector index.

The phonon self-energy is the sum of several contributions arising from different elementary mechanisms, conveniently represented by diagrams. The diagrammatic technique is given in many books and review articles.[1-6,9,10] The diagrams of interest for the calculation of phonon self-energy up to fourth order in the expansion parameter λ are shown in Fig. 1.

For convenience we list below the contributions to the self-energy of the diagrams of Fig. 1. The contribution of the second-order diagram (a) involves the product of two cubic terms of the potential, each of order λ, and therefore is of order λ^2 and is given by

$$S^{(a)}(i\omega_m) = -18\beta \sum_{q_1,q_2} |V_3(0j,q_1,q_2)|^2 \times \sum_n G_1^0(i\omega_n) G_2^0(i\omega_m - i\omega_n) . \tag{5a}$$

All other contributions arise from fourth-order diagrams involving either two quartic or one quartic and two cubic or four cubic terms of the potential. Since cubic terms are of order λ and quartic terms of order λ^2, all contributions are of order λ^4. They are given by

$$S^{(b)}(i\omega_m) = -96\beta^2 \sum_{q_1,q_2,q_3} |V_4(0j,q_1,q_2,q_3)|^2 \sum_{n,r} G_1^0(i\omega_n) G_2^0(i\omega_r) G_3^0(i\omega_m - i\omega_n - i\omega_r) , \tag{5b}$$

$$S^{(c)}(i\omega_m) = -360\beta^2 \sum_{q_1,q_2,q_3} V_3(0j,q_1,q_2) V_5(0j,-q_1,-q_2,q_3,-q_3) \sum_{n,r} G_1^0(i\omega_n) G_2^0(i\omega_m - i\omega_n) G_3^0(i\omega_r) , \tag{5c}$$

$$S^{(d)}(i\omega_m) = -216\beta^3 \sum_{q_1,q_2,q_3,q_4} V_3(0j,q_3,q_4) V_4(q_1,q_2,-q_3,-q_4) V_3(0j,-q_1,-q_2) \times \sum_{n,r} G_1^0(i\omega_n) G_2^0(i\omega_m - i\omega_n) G_3^0(i\omega_r) G_4^0(i\omega_m - i\omega_r) , \tag{5d}$$

$$S^{(e)}(i\omega_m)=-432\beta^3\sum_{q_1,q_2,q_3,q_4}V_3(0j,q_1,q_4)V_4(-q_1,q_3,-q_3,q_2)\times V_3(0j,-q_2,-q_4)\sum_{n,r}G_1^0(i\omega_n)G_2^0(i\omega_n)G_3^0(i\omega_r)G_4^0(i\omega_m-i\omega_n)\ , \tag{5e}$$

$$S^{(f)}(i\omega_m)=-432\beta^3\sum_{q_1,q_2,q_3,q_4}V_4(0j,q_1,q_2,q_3)V_3(-q_1,-q_2,q_4)V_3(0j,-q_3,-q_4)\times\sum_{n,r}G_1^0(i\omega_n)G_2^0(i\omega_r)G_3^0(i\omega_m-i\omega_n-i\omega_r)G_4^0(i\omega_n+i\omega_r)\ , \tag{5f}$$

$$S^{(g)}(i\omega_m)=-648\beta^4\sum_{q_1,q_2,q_3,q_4,q_5}V_3(0j,q_1,q_2)V_3(-q_1,q_3,q_4)V_3(-q_3,-q_4,q_5)V_3(0j,-q_5,-q_2)\times\sum_{n,r}G_1^0(i\omega_n)G_2^0(i\omega_m-i\omega_n)G_3^0(i\omega_r)G_4^0(i\omega_n-i\omega_r)G_5^0(i\omega_n)\ , \tag{5g}$$

$$S^{(h)}(i\omega_m)=-648\beta^4\sum_{q_1,q_2,q_3,q_4,q_5}V_3(0j,q_1,q_2)V_3(-q_1,q_3,q_5)V_3(-q_2,-q_3,q_4)V_3(0j,-q_4,-q_5)\times\sum_{n,r}G_1^0(i\omega_n)G_2^0(i\omega_m-i\omega_n)G_3^0(i\omega_n-i\omega_r)G_4^0(i\omega_m-i\omega_r)G_5^0(i\omega_r)\ . \tag{5h}$$

We recall that each sum over a q label is a double sum, one over the branch j and one over the phonon wave vector k. The evaluation of the various contributions to Γ^j is actually an impossible computational task. It involves multiple Brillouin-zone summations, going up to fivefold. This is further complicated by the double sum over n and r for several phonon propagators and by simultaneous summations over large number of j branches. In the case of CO_2 these are 20 in number. In the present work, we reduced this task appreciably by restricting **k** sums to a single special point only, taken as representative of the complete Brillouin zone. This **k** point was chosen so that the linewidths obtained in the lowest order when calculated using only a single point did not differ significantly from those obtained previously by using the whole scan of the BZ. This **k** point [which was found to be **k**=(0.1667,0.3333,−0.3333)] was then used in the subsequent calculation for estimating all the higher-order terms of Eqs. (5). The j summations were instead carried out over all the j branches.

The next step is that of obtaining expressions for the phonon propagators, which were given only in a formal way in Eqs. (5). In these, a double summation over n and r has yet to be made. For some of these contributions [$S^{(a)}(i\omega_m)$, $S^{(b)}(i\omega_m)$, $S^{(c)}(i\omega_m)$, $S^{(d)}(i\omega_m)$] this has been already done in Ref. 10, whereas, for others, complete expressions are not available. To obtain the contributions to the self-energy we made use of the following exact sums:

$$G_j^0(i\omega_n)=\frac{1}{\hbar\beta}\frac{2\omega_j}{(\omega_j^2+\omega_n^2)}\ , \tag{6a}$$

$$\sum_n G_j^0(i\omega_n)=2n_j+1\ , \tag{6b}$$

$$\sum_n G_1^0(i\omega_n)G_2^0(i\omega_m-i\omega_n)=F_3(i\omega_m,\omega_1,\omega_2)\ , \tag{6c}$$

$$\sum_{n,r}G_1^0(i\omega_n)G_2^0(i\omega_r)G_3^0(i\omega_m-i\omega_n-i\omega_r)=F_4(i\omega_m,\omega_1,\omega_2,\omega_3)\ , \tag{6d}$$

where

$$F_3(i\omega_m,\omega_1,\omega_2)=(1+n_1+n_2)\left[\frac{1}{(i\omega_m-\omega_1-\omega_2)}-\frac{1}{(i\omega_m+\omega_1+\omega_2)}\right]+(n_2-n_1)\left[\frac{1}{(i\omega_m-\omega_1+\omega_2)}-\frac{1}{(i\omega_m+\omega_1-\omega_2)}\right]\ , \tag{7a}$$

and

$$F_4(i\omega_m,\omega_1,\omega_2,\omega_3)=[(1+n_1)(1+n_2)(1+n_3)-n_1n_2n_3]\left[\frac{1}{(i\omega_m-\omega_1-\omega_2-\omega_3)}-\frac{1}{(i\omega_m+\omega_1+\omega_2+\omega_3)}\right]+3(n_1n_3+n_2n_3+n_3-n_1n_2)\left[\frac{1}{(i\omega_m-\omega_1-\omega_2+\omega_3)}-\frac{1}{(i\omega_m+\omega_1+\omega_2-\omega_3)}\right]\ , \tag{7b}$$

where for simplicity 1, 2, and 3 mean q_1, q_2, and q_3, respectively, and where n_j is the statistical average of the occupa-

tion number of the corresponding phonon.

Equations (7) cannot be used directly for summations over n and r in Eqs. (6a)–(6d) since these involves coupled free-phonon propagators and it is therefore necessary to make some approximation. We have found it convenient to approximate these sums by taking out an average value of the coupled free-phonon propagators, and sum over the remaining part exactly. In this approximate manner, it is possible to obtain closed forms for all the contributions from the diagrams of Fig. 1. We explain our procedure by summing over n and r for one of such complicated contributions, e.g., that of Eq. (5g). The free-phonon propagator sum in this contribution can be written, using Eqs. (6), as

$$\sum_{n,r} G_1^0(i\omega_n)G_2^0(i\omega_m-i\omega_n)G_3^0(i\omega_r)G_4^0(i\omega_n-i\omega_r)G_5^0(i\omega_n)=\sum_n G_1^0(i\omega_n)G_2^0(i\omega_m-i\omega_n)G_5^0(i\omega_n)F_3(i\omega_n,\omega_3,\omega_4)$$
$$\simeq G_5^0(i\Omega_n)F_3(i\Omega_n,\omega_3,\omega_4)F_3(i\omega_m,\omega_1,\omega_2)\ , \tag{8}$$

where Ω denotes the average value of ω. $G_j^0(i\Omega_n)$, $F(i\Omega_n,\omega_3,\omega_4)$, and $F(i\omega_n,\omega_1,\omega_2)$ are straightforwardly obtained from Eqs. (6a) and (7a), respectively. In this way, it is easy to write expressions for all contributions to the widths in a closed form. We obtain

$$\Gamma^{(a)}=18\hbar^{-2}\sum_{q_1,q_2}|V_3(0j,q_1,q_2)|^2\,\mathrm{Im}[F_3(i\omega_m,\omega_1,\omega_2)]\ , \tag{9a}$$

$$\Gamma^{(b)}=96\hbar^{-2}\sum_{q_1,q_2,q_3}|V_4(0j,q_1,q_2,q_3)|^2\,\mathrm{Im}[F_4(i\omega_m,\omega_1,\omega_2,\omega_3)]\ , \tag{9b}$$

$$\Gamma^{(c)}=360\hbar^{-2}\sum_{q_1,q_2,q_3}V_3(0j,q_1,q_2)V_5(0j,-q_1,-q_2,q_3,-q_3)(2n_3+1)\mathrm{Im}[F_3(i\omega_m,\omega_1,\omega_2)]\ , \tag{9c}$$

$$\Gamma^{(d)}=216\hbar^{-3}\sum_{q_1,q_2,q_3,q_4}V_3(0j,q_3,q_4)V_4(q_1,q_2,-q_3,-q_4)V_3(0j,-q_1,-q_2)\mathrm{Im}[F_3(i\omega_m,\omega_1,\omega_2)F_3(i\omega_m,\omega_3,\omega_4)]\ , \tag{9d}$$

$$\Gamma^{(e)}=432\hbar^{-3}\sum_{q_1,q_2,q_3,q_4}V_3(0j,q_1,q_4)V_4(-q_1,q_3,-q_3,q_2)V_3(0j,-q_2,-q_4)(2n_3+1)\left[\frac{2\omega_2}{(\omega_2^2+\Omega_n^2)}\right]\mathrm{Im}[F_3(i\omega_m,\omega_1,\omega_4)]\ , \tag{9e}$$

$$\Gamma^{(f)}=432\hbar^{-3}\sum_{q_1,q_2,q_3,q_4}V_4(0j,q_1,q_2,q_3)V_3(-q_1,-q_2,q_4)V_3(0j,-q_3,-q_4)\left[\frac{2\omega_4}{(\omega_4^2+\Omega_n^2)}\right]\mathrm{Im}[F_4(i\omega_m,\omega_1,\omega_2,\omega_3)]\ , \tag{9f}$$

$$\Gamma^{(g)}=648\hbar^{-4}\sum_{q_1,q_2,q_3,q_4,q_5}V_3(0j,q_1,q_2)V_3(-q_1,q_3,q_4)V_3(-q_3,-q_4,q_5)V_3(0j,-q_5,-q_2)$$
$$\times\left[\frac{2\omega_5}{(\omega_5^2+\Omega_n^2)}\right]F_3(i\Omega_m,\omega_3,\omega_4)\mathrm{Im}[F_3(i\omega_m,\omega_1,\omega_2)]\ , \tag{9g}$$

$$\Gamma^{(h)}=648\hbar^{-4}\sum_{q_1,q_2,q_3,q_4,q_5}V_3(0j,q_1,q_2)V_3(-q_1,q_3,q_5)V_3(-q_2,-q_3,q_4)V_3(0j,-q_4,-q_5)$$
$$\times\left[\frac{2\omega_3}{(\omega_3^2+\Omega_n^2)}\right]\mathrm{Im}[F_3(i\omega_m,\omega_1,\omega_2)F_3(i\omega_m,\omega_4,\omega_5)]\ . \tag{9h}$$

In all expressions given above momentum conservation holds. At each vertex in the diagrams of Fig. 1 this condition requires $\sum_i \mathbf{k}_i=0$. The further condition that a single $\mathbf{k}$ vector is representative of the sum in the whole Brillouin zone restricts the matrix elements involving the optical phonon $(0j)$ to only terms of the type $V_3(0j,\mathbf{k}j_1,-\mathbf{k}j_2)$ and $V_4(0j,\mathbf{k}j_1,-\mathbf{k}j_2,0j)$. For other matrix elements which do not involve the $(0j)$ phonon as those of the type $V_4(-\mathbf{k}_1j_1,\mathbf{k}_3j_3,-\mathbf{k}_3j_3,\mathbf{k}_2j_2)$ occurring in Eq. (9e), we used the average value

$$\langle V_4(-\mathbf{k}_1j_1,\mathbf{k}_3j_3,-\mathbf{k}_3j_3,\mathbf{k}_2j_2\rangle$$
$$=(1/N)\sum_{j_1,j_2,j_3}V_4(0j_1,\mathbf{k}j_3,-\mathbf{k}j_3,0j_2)\ , \tag{10}$$

where N is the appropriate normalization factor.

Before closing this section we notice that, in addition to the diagrams of Fig. 1, there are two other fourth-order diagrams that were not considered in the previous discussion. These two diagrams,

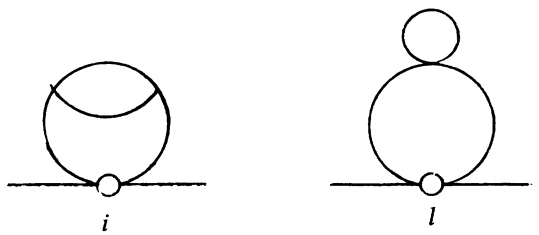

both give zero contribution to the phonon bandwidth if

the standard technique of phonon lines renormalization is used. If, however, the fluctuations of the thermal bath are taken into account diagram *i* gives a contribution to the bandwidth whereas diagram *l* is still not effective. In the next section we give an estimate of the contribution of diagram *i* and we show that this contribution is 1 order of magnitude smaller than those of the others.

III. NUMERICAL CALCULATIONS

CO_2 crystallizes in the cubic system, space group Pa3 (T_h^6) with four molecules per unit cell. The crystal possesses, in addition to the three acoustic branches, seven optical lattice branches. At the zone center these modes classify as three librational phonons (E_g, T_g^-, T_g^+) active in Raman, two translational phonons (T_u^-, T_u^+) active in infrared, and two translational phonons (A_u, E_u) inactive in both spectra.

The bandwidth of the three Raman-active lattice phonons have been first measured by Schmidt and Daniels[11] at constant volume and more recently by Ranson *et al.*[8] at constant pressure under high resolution using a tandem interferometer-spectrometer instrument in the range 6–130 K. No bandwidth data exist instead for the other phonons.

As discussed before, Procacci *et al.*[7] have calculated the contribution of three-phonon processes to the bandwidths of the lattice phonons of CO_2 with three different intermolecular potentials. In particular they produced an intermolecular potential (PRC-2), including atom-atom and charge-charge interactions, which reproduces very well the residual bandwidths at $T \simeq 0$ for the three Raman-active phonons and which predicts reasonable widths for the other four phonons as well as small anharmonic shifts. The charge distribution in the molecules was mimicked by three positive charges on the molecular axis and by exagons of negative charges around the C—O bonds. The parameters of the PRC-2 potential of Ref. 7 are listed in Table I.

TABLE I. PRC-2 intermolecular potential for crystalline CO_2.

	Atom-atom potential $V = A\exp(-Br) - Cr^{-6}$ [a]		
	A	B	C
O—O	9607	2.924	720.7
C—O	14004	3.404	271.3
R_{C-O}	0.85[b]		
	Electrostatic potential $V = q_1q_2/r$ [c]		
q_1 [d]	−0.8232		
q_2	0.1519		
r_1	1.0743		
r_2	1.5232		

[a] Units of kcal/mole and Å.
[b] In units of Å.
[c] q in units of electron charge (e); r in Å.
[d] The q_1 charge is divided into six equal charges distributed on a regular hexagon at distance $d = 0.3$ Å from the axis.

Using this potential and following the procedure described in the previous section, we have calculated the contributions to the bandwidths of all diagrams of Fig. 1 involving up to quartic terms of the intermolecular potential. The only diagram that has been neglected is thus diagram *c* which includes a V_5 term, since on one hand the calculation of the Fourier transform of fifth derivatives of the potential is extremely complex and on the other hand its contribution to the bandwidths is expected to be very small for a rapidly converging potential. We shall justify later the validity of neglecting this diagram, when we discuss the convergence of the PRC-2 potential.

Calculations were made at constant volume for five different temperatures in the range 5–150 K, using the extrapolated unit-cell parameters at $T=0$ given in Ref. 7. In principle constant pressure data should be compared to constant pressure calculations including in these the effect of the thermal expansion of the crystal. Such calculations are very involved and not feasible for the mo-

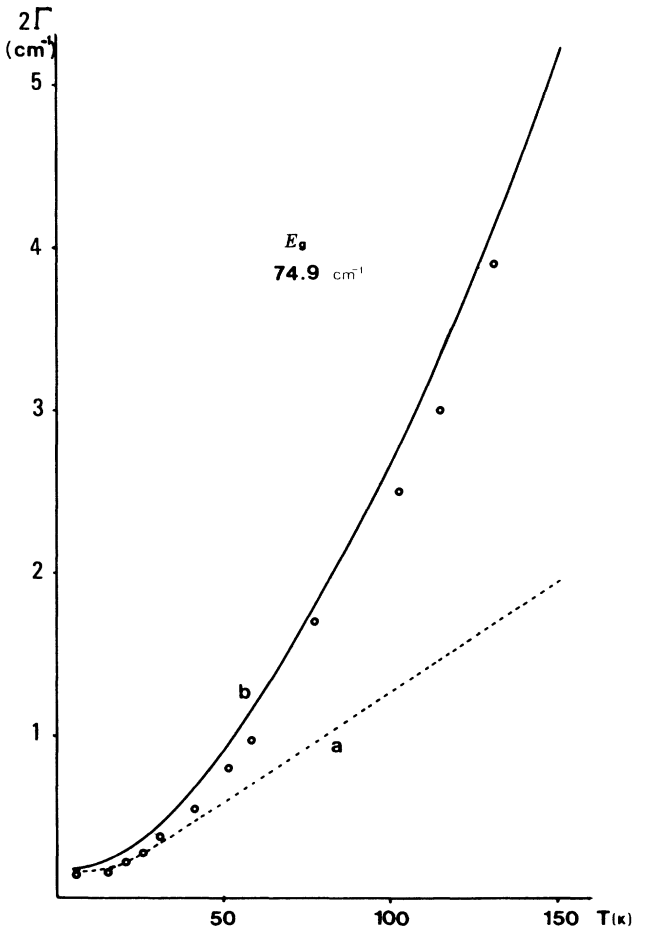

FIG. 2. Temperature dependence of the linewidth of the T_g^+ phonon. Open circles: experimental data (Ref. 8); *a*, calculated including only the lowest-order term [diagram (a)]. *b*, Calculated including the terms corresponding to diagrams (a)–(h) of Fig. 1.

ment even with large computational facilities. In order to ascertain whether or not our comparison is still meaningful, we have done a calculation of the phonon bandwidths at the temperature of 85 K, where the unit-cell volume is known,[7] assuming only three-phonon processes. This calculation produced bandwidths with negligible differences from those calculated at constant volume. A previous paper[8] discusses in detail the discrepancies existing between the constant pressure data and the constant volume data of Schmidt and Daniels,[11] showing that these are essentially due to the deconvolution technique utilized by the last authors. For these reasons we have utilized the data of Ref. 8 for comparison with our calculations.

The calculated contributions to the bandwidths are reported in Table II. For the three Raman-active phonons we compare in Figs. 2–4 the experimental bandwidths with the curves calculated using only three-phonon processes[7] (curves *a*) and with those obtained by adding to these the contributions of higher-order processes (curves *b*). The figures show very clearly the importance of the higher-order terms. The first type of curves fit the experimental data only at low temperatures and diverge considerably from them at higher temperatures. The second set of curves correctly reproduce instead the nonlinear temperature evolution of the bandwidths in the full temperature range considered. Even without stressing too much the agreement obtained, it is certainly very satisfactory to notice that the fit is better than the most optimistic prediction. Actually the experimental data are perfectly

TABLE II. Contributions to the half-width Γ (cm^{-1}) of the optical phonons at various temperatures, resulting from diagrams (a)–(h) of Fig. 1, calculated with the PRC-2 potential.

Mode	T (K)	(a)	(b)	(d)	(e)	(f)	(g)	(h)	Total
T_g^+	5.0	0.85	0.00	−0.07	0.17	0.00	0.16	−0.13	0.97
	30.0	0.98	0.00	−0.08	0.19	0.00	0.20	−0.15	1.14
	60.0	1.34	0.01	−0.14	0.32	0.02	0.39	−0.25	1.68
	100.0	2.01	0.02	−0.29	0.65	0.05	0.87	−0.51	2.80
	150.0	2.87	0.04	−0.58	1.30	0.14	1.80	−1.02	4.55
T_u^+	5.0	1.30	0.00	−0.10	0.28	0.00	0.27	−0.21	1.54
	30.0	1.54	0.00	−0.12	0.33	0.00	0.35	−0.25	1.84
	60.0	2.32	0.01	−0.23	0.57	0.03	0.71	−0.48	2.93
	100.0	3.56	0.02	−0.50	1.18	0.10	1.62	−1.04	4.94
	150.0	5.14	0.06	−1.03	2.38	0.23	3.39	−2.13	8.04
A_u	5.0	0.41	0.00	−0.02	0.05	0.00	0.05	−0.04	0.44
	30.0	0.56	0.00	−0.02	0.06	0.01	0.06	−0.05	0.61
	60.0	0.92	0.03	−0.05	0.10	0.05	0.12	−0.10	1.07
	100.0	1.46	0.09	−0.11	0.21	0.17	0.29	−0.23	1.88
	150.0	2.14	0.22	−0.22	0.43	0.40	0.60	−0.48	3.09
E_u	5.0	0.24	0.00	−0.03	0.07	0.00	0.07	−0.06	0.31
	30.0	0.41	0.00	−0.03	0.09	0.01	0.10	−0.07	0.50
	60.0	0.79	0.02	−0.06	0.17	0.04	0.22	−0.14	1.02
	100.0	1.31	0.05	−0.14	0.37	0.14	0.51	−0.32	1.90
	150.0	1.97	0.12	−0.30	0.75	0.33	1.07	−0.68	3.27
T_g^-	5.0	0.11	0.00	−0.02	0.06	0.00	0.06	−0.04	0.18
	30.0	0.20	0.00	−0.02	0.08	0.01	0.09	−0.06	0.29
	60.0	0.40	0.01	−0.05	0.16	0.04	0.20	−0.12	0.64
	100.0	0.66	0.05	−0.11	0.34	0.15	0.47	−0.27	1.28
	150.0	0.98	0.11	−0.24	0.69	0.37	1.00	−0.56	2.35
T_u^-	5.0	0.09	0.00	0.00	0.01	0.00	0.01	0.00	0.10
	30.0	0.18	0.00	0.00	0.02	0.00	0.02	−0.01	0.21
	60.0	0.37	0.02	0.00	0.04	0.03	0.05	−0.01	0.50
	100.0	0.64	0.07	−0.01	0.09	0.10	0.13	−0.02	1.01
	150.0	0.98	0.16	−0.01	0.20	0.25	0.29	−0.03	1.82
E_g	5.0	0.08	0.00	0.00	0.01	0.00	0.01	−0.01	0.09
	30.0	0.17	0.01	0.00	0.02	0.01	0.02	−0.01	0.22
	60.0	0.36	0.04	0.00	0.07	0.05	0.09	−0.01	0.59
	100.0	0.63	0.12	0.00	0.18	0.16	0.24	−0.01	1.33
	150.0	0.97	0.30	0.00	0.39	0.39	0.55	−0.01	2.58

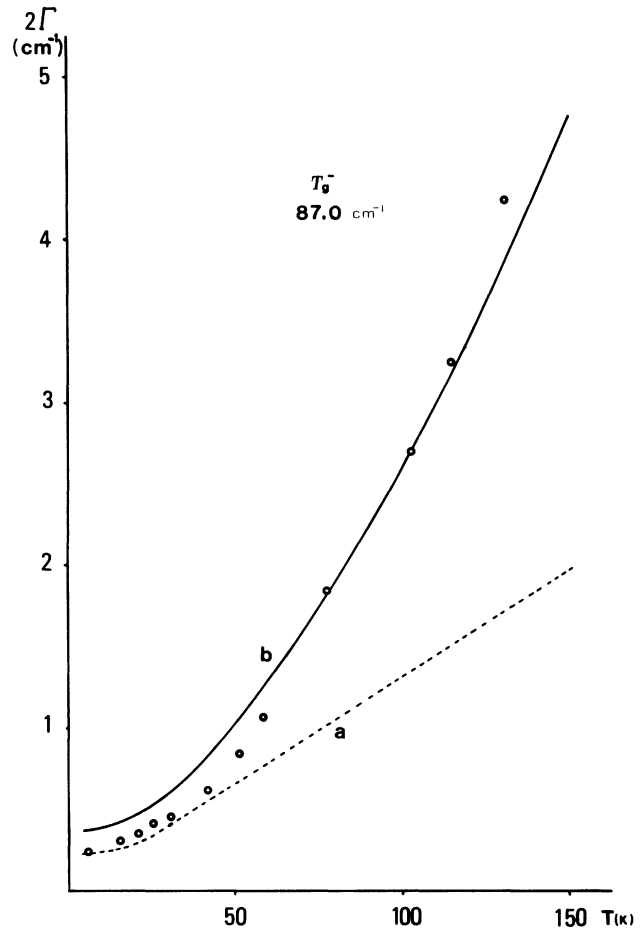

FIG. 3. Temperature dependence of the linewidth of the T_g^- phonon. See caption to Fig. 2.

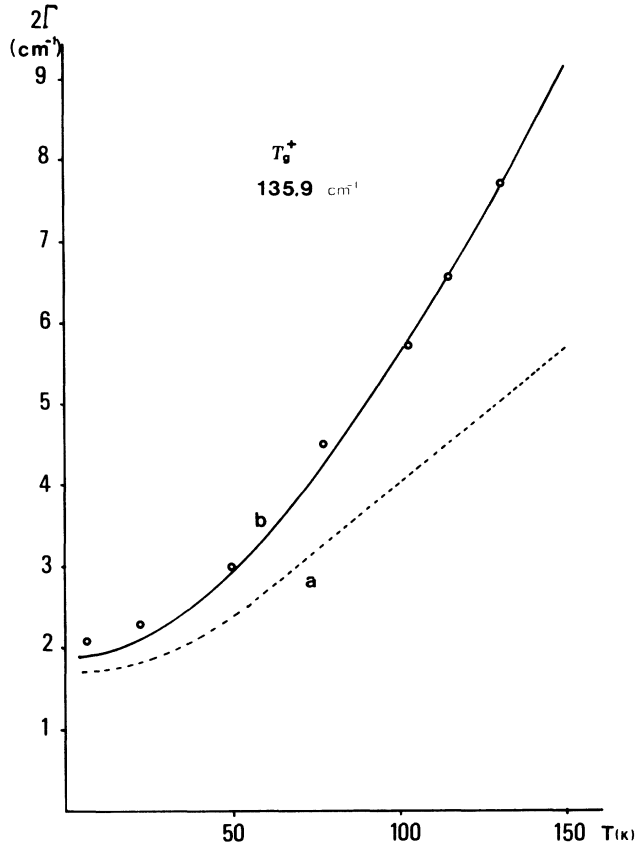

FIG. 4. Temperature dependence of the linewidth of the E_g phonon. See caption to Fig. 2.

reproduced for the T_g^+ phonon and with small differences for the E_g phonon. Only in the case of the T_g^- phonon the calculated curve seems to have a less steeper slope than the experimental data. Processes higher than the lowest-order three-phonon decays of diagram *a* are thus not negligible, as often assumed, except that at very low temperatures where the thermal bath is almost completely depopulated. At higher temperatures their contribution is instead of the same order of magnitude or even larger than that due to three-phonon decay processes. In Table III we report the average values of the cubic and quartic coupling coefficients used in the present work. This table shows that the cubic coupling terms are in average constant with the phonon frequency whereas the quartic terms decrease when the phonon frequency increases.

We now discuss in some detail the different diagrams of Fig. 1. The analysis of their contributions to the bandwidths, given by Eqs. (9a)–(9h), shows that they can be classified in three groups.

(i) Diagrams (a), (e), and (g) whose contribution depends on the function $F_3(i\omega_m,\omega_i,\omega_j)$ and increases with increasing frequency. These processes represent three-phonon decay mechanisms and differ only because of the different coupling of the intermediate phonons with the thermal bath. The increase of the contribution with increasing phonon frequency can be easily understood on the basis of the average anharmonic coefficients given in Table III. The V_3 terms of the potential are in fact practically independent on the phonon frequency: as a result, the anharmonic terms of diagrams (a), (e), and (g), which are dominated by the cubic anharmonicity, depend essentially on the number of possible decay channels,[7] thus increasing with increasing phonon frequency.

(ii) Diagrams (b) and (f) whose contribution involves the function $F_4(i\omega_m,\omega_i,\omega_j,\omega_k)$ and behave thus as four-phonon processes. Their contribution to the overall bandwidth is very small for all phonons and decreases as the phonon frequency increases. Table III shows that the

TABLE III. Average anharmonic coupling coefficients for the optical phonons of solid CO_2 (PRC-2 potential).

Mode	ω	$\lvert V_3 \rvert$	V_4
T_g^+	135.9	0.274×10^{-2}	0.931×10^{-3}
T_u^+	118.4	0.369×10^{-2}	0.884×10^{-3}
A_u	103.3	0.268×10^{-2}	0.156×10^{-2}
E_u	92.4	0.445×10^{-2}	0.115×10^{-2}
T_g^-	87.0	0.428×10^{-2}	0.118×10^{-2}
T_u^-	75.2	0.214×10^{-2}	0.135×10^{-2}
E_g	74.9	0.320×10^{-2}	0.154×10^{-2}

V_4 potential terms are larger for the low-frequency phonons; thus the same is true for the contributions of diagrams (b) and (f) which are essentially controlled by the quartic anharmonicity. Even if the contribution is small in the temperature range considered, it is worth discussing the relaxation mechanisms described by the fourth-order diagram (b). Its contribution to the half-bandwidth is given by[6]

$$\Gamma^b = 96\hbar^{-2} \sum_{q_1,q_2,q_3} |V_4(0j,q_1,q_2,q_3)|^2 \{[(n_1+1)(n_2+1)(n_3+1)-n_1n_2n_3]\delta(\omega_m-\omega_1-\omega_2-\omega_3)$$
$$+3[n_1(n_2+1)(n_3+1)-(n_1+1)n_2n_3]\delta(\omega_m+\omega_1-\omega_2-\omega_3)$$
$$+3[n_1n_2(n_3+1)-(n_1+1)(n_2+1)n_3]\delta(\omega_m+\omega_1+\omega_2-\omega_3)\} . \quad (11)$$

TABLE IV. Contributions to damping of different decay processes corresponding to diagram *b* (see text).

Mode	T (K)	Down	%	Up	%	Total	%	Up-down Pure dephas.	%	Total
T_g^+	5	0.0002	100.0	0.0000	0.0	0.0000	0.0	0.0000	0.0	0.0002
	30	0.0003	27.1	0.0000	0.0	0.0007	74.0	0.0005	52.1	0.0010
	60	0.0004	7.7	0.0000	0.6	0.0051	92.8	0.0033	61.5	0.0054
	100	0.0008	4.9	−0.0001	0.5	0.0162	95.7	0.0105	62.2	0.0169
	150	0.0016	4.1	−0.0002	0.5	0.0381	96.5	0.0247	62.5	0.0395
T_u^+	5	0.0002	100.0	0.0000	0.0	0.0000	0.0	0.0000	0.0	0.0002
	30	0.0002	15.2	0.0000	0.0	0.0010	84.8	0.0005	49.1	0.0011
	60	0.0003	3.6	0.0000	0.4	0.0072	96.8	0.0037	49.1	0.0074
	100	0.0005	2.2	−0.0001	0.4	0.0234	98.2	0.0115	48.4	0.0238
	150	0.0010	1.8	−0.0003	0.4	0.0554	98.6	0.0270	48.1	0.0562
A_u	5	0.0004	100.0	0.0000	0.0	0.0000	0.0	0.0000	0.0	0.0004
	30	0.0004	11.3	0.0000	0.3	0.0034	89.0	0.0016	42.3	0.0038
	60	0.0007	2.4	−0.0001	0.4	0.0276	98.0	0.0115	40.7	0.0282
	100	0.0013	1.4	−0.0004	0.4	0.0916	99.0	0.0370	40.0	0.0925
	150	0.0025	1.1	−0.0010	0.4	0.2185	99.3	0.0874	39.7	0.2200
E_u	5	0.0002	100.0	0.0000	0.0	0.0000	0.0	0.0000	0.0	0.0002
	30	0.0002	10.0	0.0000	0.5	0.0020	90.5	0.0014	63.3	0.0022
	60	0.0004	2.2	−0.0001	0.4	0.0157	98.2	0.0095	59.4	0.0160
	100	0.0007	1.3	−0.0003	0.5	0.0520	99.2	0.0302	57.5	0.0524
	150	0.0013	1.1	−0.0006	0.5	0.1240	99.4	0.0709	56.9	0.1247
T_g^-	5	0.0002	100.0	0.0000	0.0	0.0000	0.0	0.0000	0.0	0.0002
	30	0.0002	9.9	0.0000	0.6	0.0015	90.1	0.0007	41.9	0.0017
	60	0.0003	1.9	−0.0001	0.5	0.0138	98.6	0.0056	40.2	0.0140
	100	0.0005	1.1	−0.0002	0.5	0.0472	99.4	0.0187	39.4	0.0475
	150	0.0010	0.8	−0.0006	0.5	0.1138	99.6	0.0448	39.2	0.1143
T_u^-	5	0.0002	100.0	0.0000	0.0	0.0000	0.0	0.0000	0.0	0.0002
	30	0.0002	8.4	0.0000	0.4	0.0023	92.0	0.0010	41.8	0.0025
	60	0.0003	1.7	−0.0001	0.5	0.0198	98.9	0.0084	41.9	0.0200
	100	0.0006	1.0	−0.0004	0.6	0.0668	99.7	0.0280	41.8	0.0671
	150	0.0012	0.8	−0.0010	0.6	0.1604	99.8	0.0671	41.7	0.1607
E_g	5	0.0003	100.0	0.0000	0.0	0.0000	0.0	0.0000	0.0	0.0003
	30	0.0004	7.2	0.0000	0.6	0.0049	93.3	0.0024	46.3	0.0052
	60	0.0006	1.6	−0.0002	0.6	0.0379	99.0	0.0163	42.4	0.0383
	100	0.0013	1.0	−0.0007	0.6	0.1242	99.6	0.0515	41.3	0.1248
	150	0.0025	0.8	−0.0017	0.6	0.2950	99.7	0.1210	40.9	0.2958

The first term describes a down-conversion process in which the optical phonon decays into three phonons of lower energy, the second an up-down process in which a phonon of the thermal bath is fused with the optical phonon to produce two phonons, and the third an up-conversion process in which two phonons of the bath combine with the optical phonon to give rise to a higher-energy phonon. These different processes are schematically represented below by the diagrams b_{down}, $b_{\text{up-down}}$, and b_{up}, respectively.

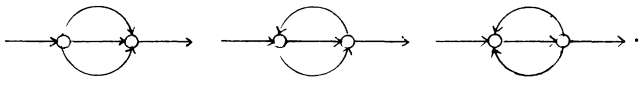

b_{down} $b_{\text{up-down}}$ b_{up}

A special case of the up-down process is that in which the annihilated and created phonons ω_1 and ω_2 are the same and the other created phonon ω_2 is the optical phonon ω_m itself. This corresponds to a pure dephasing process which contributes to the width without changing the phonon occupation numbers. The separate contributions of the three decay and of the pure dephasing processes are shown in Table IV. The up-down conversion process is by far the most important one and about one-half of its contribution is due to the pure dephasing process.

(iii) Diagrams (d) and (h) whose contribution involves produces of the type $F_3(i\omega_m,\omega_i,\omega_j)F_3(i\omega_m,\omega_k,\omega_l)$ and increases with increasing phonon frequency. In contrast to all other diagrams these give rise to negative contributions to the bandwidth. Such a result can be, however, easily understood by considering expressions (9d) and (9h) for the half-bandwidths. As pointed out before, both equations include the imaginary part of products of two complex quantities of the type $\Delta_{ij}+i\Gamma_{ij}$. The real part of $F_3(i\omega_m,\omega_i,\omega_j)$ is the anharmonic frequency shift and the imaginary part the damping. The bandwidth will be then proportional to

$$\begin{aligned}&\mathrm{Im}[F_3(i\omega_m,\omega_i,\omega_j)F_3(i\omega_m,\omega_k,\omega_l)]\\&\quad=\mathrm{Im}[(\Delta_{ij}+i\Gamma_{ij})(\Delta_{kl}+i\Gamma_{kl})]\\&\quad=(\Delta_{ij}\Gamma_{kl})+(\Delta_{lk}\Gamma_{ij})\end{aligned}\tag{12}$$

which shows that in both cases the contribution to the width, due to the phonons ω_i and ω_j is modulated by the frequency shift due to the phonons ω_k and ω_l and vice versa. Previous calculations have shown that cubic shifts are normally negative: therefore, the terms $\Delta_{ij}\Gamma_{kl}$ and $\Delta_{kl}\Gamma_{ij}$ will contribute negatively to the bandwidth. The occurrence of negative contributions for these diagrams is simply a consequence of the perturbation technique. At each level of perturbation, it is only the total contribution to the bandwidths of all elementary diagrams which is physically meaningful and must therefore be always positive and not necessarily that of the individual ones.

We discuss now briefly the validity of the PRC-2 potential used in our calculations. In Table V we report the average values of the coupling coefficients $\langle V_3\rangle^2$, $\langle V_4\rangle$, $\langle V_3\rangle^2\langle V_4\rangle$, and $\langle V_3\rangle^4$ for the PRC-2 as well as for the more anharmonic PRC-1 potential of Ref. 7. The coupling coefficients $\langle V_3\rangle^2$ and $\langle V_4\rangle$ are about the same for the PRC-1 potential while the quartic anharmonic coefficient is smaller than $\langle V_3\rangle^2$ for the PRC-2 potential. We consider this as an indication that the anharmonic expansion is a fast converging series for the PRC-2 potential; as a consequence terms of the type V_3V_5, occurring in the contribution of diagram c, are expected to be smaller than those of the type $V_3^2V_4$ or V_3^4. Diagram (c), not included in the present calculation is thus expected to bring a minor contribution to the total bandwidths.

We conclude therefore that the PRC-2 potential has the right degree of anharmonicity and the correct convergence to reproduce correctly the complete dynamical behavior of the CO_2 crystal up to the fourth-order perturbation level. Unfortunately no data exist for the bandwidths of the infrared active phonons and it would certainly be interesting to dispose of these to see if our predictions are correct.

In the previous section we have discussed the fact that diagram i gives rise to a contribution to the width if the fluctuations of the thermal bath are taken into account.[12] We have estimated this contribution using the approximate expression

$$\Gamma^i=\beta\Delta_1(T)\langle n_1\rangle\langle\Gamma_1\rangle+\tfrac{1}{2}\beta[\Delta_1(T)-\Delta_1(0)]\langle\Gamma_1\rangle\tag{13}$$

obtained by simply introducing the complex anharmonic frequency of the scattering phonon ω_1 in the expression for occupation number occurring in the self-energy of diagram i. We found that, at the temperature of 80 K, this contribution is of the order of 0.005–0.015 cm^{-1}, depending on the phonon considered, and goes to zero as T goes to 0. For this reason we have neglected it in our calculations. A more complete evaluation of this contribution will be presented in a forthcoming paper.[13]

ACKNOWLEDGMENTS

This work was supported by the Italian Ministero della Pubblica Istruzione (M.P.I.) and Consiglio Nazionale delle Ricerche (CNR). One of us (V.K.J.) acknowledges the Third World Academy of Science (TWAS) for financial support.

TABLE V. Average anharmonic coefficients for PRC-1 and PRC-2 potentials.

	$\lvert V_3\rvert^2$	V_4	$\lvert V_3\rvert^2V_4$	$\lvert V_3\rvert^4$	V_4^2
PRC-1	0.429×10^{-2}	0.333×10^{-2}	0.135×10^{-4}	0.197×10^{-4}	0.128×10^{-4}
PRC-2	0.333×10^{-2}	0.117×10^{-2}	0.386×10^{-5}	0.118×10^{-4}	0.144×10^{-5}

*Permanent address: Department of Physics, Panjab University, Chandigarh 160 014, India.

[1]A. L. Fetter and J. B. Walecka, *Quantum Theory of Many Particle Systems* (McGraw-Hill, New York, 1971).

[2]D. N. Zubarev, Usp. Fiz. Nauk. **71**, 71 (1960) [Sov. Phys.—Usp. **3**, 320 (1960)].

[3]A. I. Alekseev, Usp. Fiz. Nauk. **73**, 41 (1961) [Sov. Phys.—Usp. **4**, 23 (1961)].

[4]A. A. Maradudin and A. L. Fein, Phys. Rev. **128**, 2589 (1962).

[5]S. Califano, V. Schettino, and N. Neto, *Lattice Dynamics of Molecular Crystals,* Vol. 21 of *Lecture Notes in Chemistry,* edited by G. Berthier *et al.* (Springer, New York, 1981).

[6]S. Califano and V. Schettino, Int. Rev. Phys. Chem. **7**, 19 (1988), and references therein.

[7]P. Procacci, R. Righini, and S. Califano, Chem. Phys. **116**, 171 (1987).

[8]P. Ranson, R. Ouillon, and S. Califano, J. Chem. Phys. (to be published).

[9]I. P. Ipatova, A. A. Maradudin, and R. F. Wallis, Fiz. Tverd. Tela (Leningrad) **8**, 1064 (1966) [Sov. Phys.—Solid State **8**, 850 (1966)].

[10]R. S. Tripathi and K. N. Pathak, Nuovo Cimento **21B**, 290 (1974).

[11]J. W. Schmidt and W. B. Daniels, J. Chem. Phys. **73**, 4848 (1980).

[12]S. Marks, P. A. Cornelius, and C. B. Harris, J. Chem. Phys. **73**, 3069 (1980).

[13]V. K. Jindal, F. Bogani, R. Righini, and S. Califano (unpublished).